

# Counterflow Virtual Impactor Based Collection of Small Ice Particles in Mixed-Phase Clouds for the Physico-Chemical Characterization of Tropospheric Ice Nuclei: Sampler Description and First Case Study

S. Mertes,<sup>1</sup> B. Verheggen,<sup>2,\*</sup> S. Walter,<sup>3</sup> P. Connolly,<sup>4</sup> M. Ebert,<sup>5</sup> J. Schneider,<sup>3</sup>  
K. N. Bower,<sup>4</sup> J. Cozic,<sup>2</sup> S. Weinbruch,<sup>5</sup> U. Baltensperger,<sup>2</sup> and E. Weingartner<sup>2</sup>

<sup>1</sup>Leibniz-Institute for Tropospheric Research, Leipzig, Germany

<sup>2</sup>Laboratory of Atmospheric Chemistry, Paul Scherrer Institut, Villigen PSI, Switzerland

<sup>3</sup>Max Planck Institute for Chemistry, Mainz, Germany

<sup>4</sup>University of Manchester, Manchester, United Kingdom

<sup>5</sup>Technical University Darmstadt, Darmstadt, Germany

\*Present affiliation: Energy Research Centre of the Netherlands, Petten, The Netherlands

---

A ground-based sampling system named Ice-CVI is introduced that is able to extract small ice particles with sizes between 5 and 20  $\mu\text{m}$  out of mixed-phase clouds. The instrument is based on a counterflow virtual impactor (CVI) removing interstitial particles and is supplemented by additional modules that pre-segregate other constituents of mixed-phase clouds. Ice particles of 20  $\mu\text{m}$  and smaller are expected to grow only by water vapor diffusion and there is a negligible probability that they scavenge aerosol particles by impaction and riming. Thus, their residuals which are released by the Ice-CVI can be interpreted as the original ice nuclei (IN). In a first field test within the Cloud and Aerosol Characterization Experiment (CLACE-3) at the high alpine research station Jungfraujoch, the collection behavior of the single components and the complete system was evaluated under atmospheric sampling conditions. By comparing parameters measured by the Ice-CVI with corresponding results obtained from other inlets or with in-situ instrumentation it is verified that the small ice particles are representatively collected whereas all other mixed phase cloud constituents are

effectively suppressed. In a case study it is observed that supermicrometer particles preferentially serve as IN although in absolute terms the IN concentration is dominated by sub-micrometer particles. Mineral dust (Si), non-volatile organic matter and black carbon could be identified as IN components by means of different chemical analyses. The latter suggests an anthropogenic influence on the heterogeneous ice nucleation in supercooled, tropospheric clouds.

---

## 1. INTRODUCTION

The nucleation of ice particles in middle and lower tropospheric clouds can initiate precipitation (Chen and Lamb 1999) and change cloud radiative properties (Sun and Shine 1995). Hence, ice formation influences cloud lifetime and albedo and thus affects the climate forcing of tropospheric clouds below cirrus level (Lohmann and Feichter 2005; Vali 1996).

Because temperatures in the lower and middle troposphere are essentially above the homogeneous freezing limit of about  $-40^\circ\text{C}$ , heterogeneous nucleation which is triggered by a subset of atmospheric aerosol particles, named ice nuclei (IN), initiates ice formation inside supercooled clouds. Several heterogeneous nucleation processes are recognized such as deposition, condensation nucleation and drop freezing caused by contact, immersion and evaporative freezing (Cantrell and Heymsfield 2005).

A question closely related to the different heterogeneous ice nucleation mechanisms is the nature of the IN. In the middle and lower troposphere, the chemical composition and microphysical properties of IN might be different to the physico-chemical properties of upper tropospheric IN due to specific aerosol sources and other thermodynamic conditions. In particular, the anthropogenic influence on middle and lower tropospheric ice formation is not well known.

---

Received 20 November 2006; accepted 8 June 2007.

This work is funded by the German Research Foundation (DFG, grants He 939/8-1 and He 939/8-2) and is additionally supported by MeteoSwiss (GAW Program of the WMO), the Swiss National Science Foundation (No. 200020-108032), the FP6 network of excellence ACCENT and the Natural Environment Research Council NERC (NER/A/S/2001/01135). We thank the International Foundation High Altitude Research Stations Jungfraujoch and Gornergrat (HFSJG) for the opportunity to perform experiments on the high alpine research station Jungfraujoch. Furthermore we like to thank H. Haudek, W. Sarwatka†, A. Haudek, S. Günnel and P. Glomb for the electronic and mechanical construction of the Ice-CVI and their help preparing the field measurements.

Address correspondence to S. Mertes, Leibniz-Institute for Tropospheric Research, D-04318, Leipzig, Germany. E-mail: mertes@tropos.de

A device which enables to measure the concentration, size, and chemical properties of IN, which have indeed nucleated atmospheric ice particles is the counterflow virtual impactor (CVI, Ogren et al. 1985). The CVI samples and evaporates hydrometeors above a certain size inside clouds and thereby releases dry residual particles. The airborne CVI technique was successfully deployed in cirrus clouds and contrails (e.g., Cziczo et al. 2004; Heintzenberg et al. 1996; Seifert et al. 2004; Ström and Ohlsson 1998; Twohy and Gandrud 1998; Twohy and Poellot 2005). However, a CVI cannot be applied offhand in mixed-phase clouds (co-existence of ice particles and supercooled drops), which mainly persist in the lower and middle troposphere, because the sampling system does not distinguish between frozen and liquid cloud elements of the same size. Hence, the sample is contaminated by supercooled drops. Moreover, a CVI would additionally sample rimed ice crystals and ice crystals that scavenged aerosol particles by impaction, releasing residuals in the CVI that were incorporated after ice nucleation and therefore render the IN determination ambiguous.

In order to overcome these sampling issues in mixed-phase clouds a novel ground-based inlet system, the Ice-CVI, has been designed and tested on the high alpine research station Jungfraujoch in the Swiss Alps at 3580 m asl. The prerequisite for this sampling device was to extract small, freshly formed ice particles separated from other solid/liquid components of a mixed-phase cloud (interstitial particles, supercooled drops, large ice aggregates, and precipitation particles). Ice particles grow initially by

water vapor diffusion, i.e., the residual particles of the sampled small ice particles can be interpreted as their original IN as long as riming does not become an important growth mechanism. The transition from vapor-grown to rimed ice particles is predicted for diameters larger than  $50\ \mu\text{m}$  (Chen and Lamb 1999; Fukuta and Takahashi 1999). Therefore, the main purpose of the Ice-CVI is a strict size and water phase separation of hydrometeors inside mixed-phase clouds in order to obtain information about tropospheric IN. A high and quantifiable sampling efficiency of the system for small ice particles containing IN is of secondary importance.

In the following sections, the Ice-CVI system will be described and the influence of its different components on the sampling behavior will be discussed by means of aerosol measurements downstream and cloud microphysical measurements in parallel to the Ice-CVI. Thereafter, first results of residual particles that are considered as IN will be presented.

## 2. DESIGN OF THE Ice-CVI

The Ice-CVI consists of several components that affect the sampling characteristics. The complete system is vertically aligned (Figure 1). The cloud air is aspirated by an omnidirectional, exponentially tapered horn initially 26 cm in diameter, decreasing to 4 cm over 16 cm distance. The aspiration efficiency of an identically shaped inlet with similar dimensions and also operated at crosswind conditions was determined in a wet wind tunnel by Noone et al. (1992). They found a good agreement between their experimental results and a theoretically

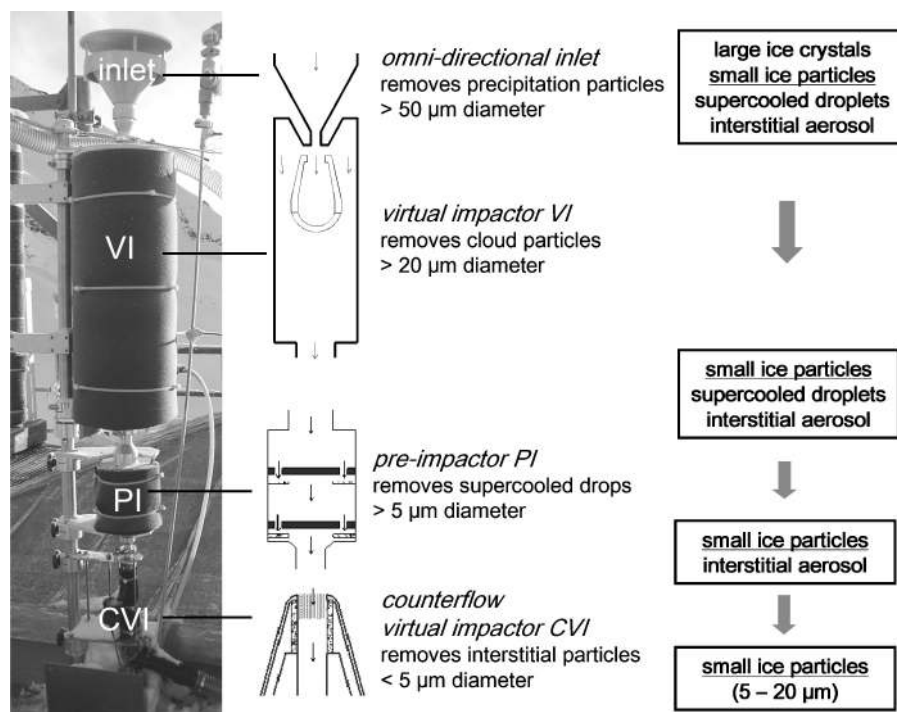


FIG. 1. Ice-CVI setup on the roof platform of the high alpine research station Jungfraujoch along with a schematic drawing describing the role of each component for the ultimate collection of small ice particles. The CVI inlet tip is installed in a wind-tunnel.

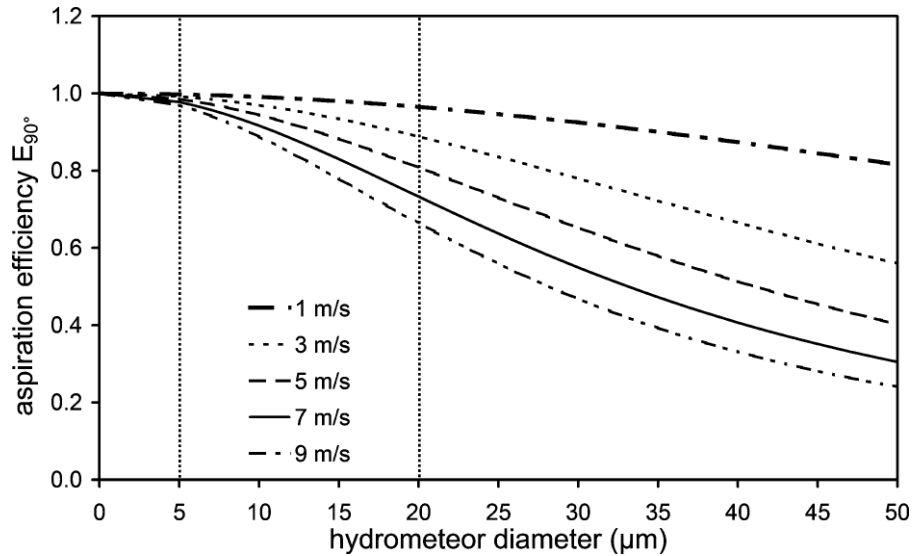


FIG. 2. Aspiration efficiency of the Ice-CVI omni-directional inlet calculated from Equation (1) as a function of hydrometeor diameter and for different wind velocities (cf. legend). Dotted lines represent the upper and lower cut-off sizes determined by the VI and CVI, respectively.

derived inlet efficiency  $E_{90^\circ}$  for  $90^\circ$  sampling given by Equation (1),

$$E_{90^\circ} = \frac{1}{1 + 4 \cdot G \cdot St \cdot R^{0.5}} \quad [1]$$

where  $R$  is the ratio of wind and inlet velocity,  $St$  is the Stokes number of the sampled hydrometeors and  $G$  is a coefficient depending on  $R$ . The maximum inlet diameter of 26 cm is used as the characteristic dimension to derive  $St$  according to Noone et al. (1992). The inlet velocity is calculated for the minimum inlet diameter of 4 cm yielding  $1.3 \text{ m s}^{-1}$  at a typical sampling flow rate of  $420 \text{ liter min}^{-1}$ . Figure 2 shows  $E_{90^\circ}$  for different horizontal wind speeds as a function of particle diameter. According to Equation (1),  $20\text{-}\mu\text{m}$  particles are sampled with an efficiency of 0.9 up to a wind velocity of  $3 \text{ m s}^{-1}$ . On the other hand it is obvious from Figure 2 that the  $90^\circ$  sampling substantially reduces the undesired collection of ice crystals larger than about  $50 \mu\text{m}$ , which is the size range where the ‘‘contamination’’ of crystals by riming and aerosol impaction scavenging becomes important.

However, during precipitation periods, the collection of much larger falling or blowing snowflakes and graupel cannot be completely prevented during  $90^\circ$  sampling, although the inlet is protected by a roof. In order to remove the precipitation or wind-blown particles inside the Ice-CVI and to ensure a controlled upper sampling size, a virtual impactor (VI) is connected downstream of the inlet horn. The VI is constructed according to the improved virtual impactor design presented by Chen and Yeh (1987). The dimensions are chosen such that particles larger than  $20 \mu\text{m}$  ( $D_{50\%}$  cut size diameter) are virtually impacted into the minor flow ( $20 \text{ liter min}^{-1}$ ), whereas smaller particles remain in the sample flow ( $400 \text{ liter min}^{-1}$ ). The upper limit of  $20 \mu\text{m}$  is reasonable, because it assures a collection efficiency of nearly 1

for all sampled ice particles up to wind velocities of  $3 \text{ m s}^{-1}$  (see Figure 2 and inlet discussion above). Moreover, the possibility of ice particle breakup is minimized by the choice of this upper size limit, which will be discussed in section 3. Measurements in mixed-phase clouds have shown that the ice particle number concentration is often dominated by ice particles with diameters below and around  $20 \mu\text{m}$  (Korolev et al. 2003; Oshchepkov et al. 2000; Turner, 2005), i.e., that a representative size range is still collected.

Downstream of the VI a pre-impactor (PI) is installed which separates the small ice particles from the supercooled drops. The latter freeze upon contact with impaction plates colder than  $0^\circ\text{C}$ , while the former bounce off and remain in the sample airflow. A two-stage design was chosen for the PI similar to the ETH cloud impactor (Collett Jr. et al. 1993). The first stage has a cut-off diameter of  $10 \mu\text{m}$  and the second of  $4 \mu\text{m}$ . The impactor concept to collect supercooled drops quantitatively by freezing on cool plates has been realized by Straub and Collett (2001). The feasibility of a liquid phase pre-segregation under mixed-phase conditions inside an inertial impactor was successfully shown by Tenberken-Pötzsch et al. (2000) and applied in atmospheric clouds by Laj et al. (2001).

The CVI itself is located downstream of the PI to reject the interstitial particles. The CVI inlet is installed inside a wind tunnel to accelerate the incoming air up to  $120 \text{ m s}^{-1}$ , which is needed to reach a  $D_{50\%}$  cut size of about  $5 \mu\text{m}$  (Schwarzenböck et al. 2000). A controlled counterflow of  $1\text{--}2 \text{ liter min}^{-1}$  is blown out of the inlet tip, which allows only hydrometeors of sufficient inertia to enter the system. Since, by this stage, the supercooled drops and larger ice crystals have already been removed by the PI and VI, respectively, it is considered that only the small ice particles ( $5 \mu\text{m} < D_{\text{ice}} < 20 \mu\text{m}$ ) are sampled, whereas the lower and upper cut-off diameters are determined by the CVI and the

VI. Inside the CVI the small ice particles are injected into a particle-free and dry carrier air (flow rate 6–12 liter  $\text{min}^{-1}$ ) for complete sublimation. No heating is applied, i.e., that the walls of the respective evaporation tube and the carrier air have room temperature. Downstream of this section the water vapor representing the sampled ice water content (IWC) and the released residual particles can be analyzed by dedicated instrumentation. The CVI sampling principle leads to an enrichment of the collected hydrometeors (and thus of the residual particles), which is essential for the determination of the expected low IN number and mass concentration. The enrichment is given by the velocity ratio upstream and downstream the CVI inlet tip. Enrichment factors between 5 and 10 were reached with our sampling and detection configuration.

The standard aerosol instrumentation downstream of the Ice-CVI consists of a condensation particle counter (CPC, TSI-3010) and a particle soot absorption photometer (PSAP) in order to measure number concentration and black carbon (BC) mass concentration of the residual particles. The PSAP is a filter-based method to determine the absorption coefficient of aerosol particles. The measured signal is corrected according to Bond et al. (1999) except for scattering in the filter matrix (which can account for 5–10% of the total signal) and then transferred to a black carbon (BC) mass concentration using an absorption efficiency of  $8.5 \text{ m}^2 \text{ g}^{-1}$  derived for aerosol particles at JFJ during winter at 580 nm (Cozic et al. 2007). The collected IWC is determined by two Lyman-alpha hygrometers and a dew point mirror. The CVI used in this study was successfully deployed in ground-based studies of warm (e.g., Mertes et al. 2001, 2005) and artificially seeded supercooled clouds (Schwarzenböck et al. 2001).

### 3. SAMPLING ISSUES

A variety of processes like deposition losses, ice crystal break-up and abrasion of stainless steel particles from the impactor surfaces might affect the sampling characteristics of the Ice-CVI. Shattering of graupel (usually several hundred micrometers in size) and ice particles larger than  $600 \mu\text{m}$  on surfaces of airborne instruments were observed at flight velocities of at least  $100 \text{ m s}^{-1}$  (Gardiner and Hallett 1985; Korolev and Isaac 2005). At the total volume flow through the Ice-CVI of  $420 \text{ liter min}^{-1}$ , the air velocities inside the impactors in front of the CVI are only  $1.3 \text{ m s}^{-1}$  at the point of virtual impaction inside the VI, and 8 and  $28 \text{ m s}^{-1}$  at the two inertial impaction plates inside the PI, respectively. This means that not only the ice particle size ( $D_{\text{ice}} \leq 20 \mu\text{m}$ ) but also the air velocities are substantially smaller than during the observations of ice particle shattering on research aircrafts. A more quantitative approach to estimate the probability of ice particle breakup inside the Ice-CVI is the determination of the kinetic to surface energy ratio  $L$  (Equation [2]; Vidaurre and Hallett 2006), where  $v$  is the impact velocity,  $m$  is the hydrometeor mass,  $A$  its surface area and  $\sigma$  the surface tension. The surface area of the small ice particles is calculated

assuming a quasi-spherical shape, which was observed by Korolev and Isaac (2003) in clouds between 0 and  $-40^\circ\text{C}$ .

$$L = \frac{1/2mv^2}{\sigma A} \quad [2]$$

A critical kinetic to surface energy ratio  $L_{\text{crit}}$  between 7 to 10 has been found in laboratory studies above which drop break up occurs (Hallett and Christensen 1984). Because empirically derived values of  $L_{\text{crit}}$  are missing for ice particles, the criterion for liquid drops is adopted by Vidaurre and Hallett (2006) using a constant surface tension (i.e., constant ice surface energy) of  $0.12 \text{ J m}^{-2}$ . However, for the small, compact ice particles inside the PI a higher  $L_{\text{crit}}$  might be expected. For the impaction inside the PI,  $L$  values of 0.2–0.7 (first stage) and 2.3–9.2 (second stage) are derived for the ice particle size range of 5–20  $\mu\text{m}$ , with the bulk ice density of  $0.91 \text{ g cm}^{-3}$  to infer the ice particle mass. Hence significant shattering seems to be unlikely. Further upstream, the few large precipitation particles that might enter the omni-directional inlet are much more subjected to shattering, but they are removed from the sample flow without any surface contact by the VI. For hydrometeors with diameters close to the  $D_{50\%}$  of the VI, which thus might have contact with the surface of the minor flow collection probe,  $L$  is calculated to be below 0.1.

The rather low impinging velocity of the small ice particles also reduces the risk for a substantial abrasion of stainless steel particles from the inner surfaces of the Ice-CVI (Murphy et al. 2004), especially from the PI impaction plates. The small ice particles only possess high velocities inside the wind tunnel in front and just behind the CVI inlet tip. Inside the wind tunnel, the CVI tip itself would be the only obstacle, but eventual fragments of the primary ice particle will not retain the initial velocity and will thus be blocked by the CVI counterflow. Potential abraded particles from the CVI tip are rejected by the counterflow as well or need to be larger than the CVI cut size of  $5 \mu\text{m}$  to be sampled and are thus easy to identify. Due to the vertical CVI setup there are no opposing surfaces or bends where abrasion of particles from the inner surfaces could occur downstream of the CVI tip, until the ice particles are decelerated to the carrier air velocity of about  $15 \text{ m s}^{-1}$ .

Thus, the most critical issue is an insufficient retention and/or low transmission of the PI with respect to supercooled drops and small ice particles. Qualitative tests were carried out in the laboratory following the methodology presented by Tenberken-Pötzsch et al. (2000). An ultrasonic nebulizer was used for drop generation and a cooling section for intermittent drop freezing upstream of the PI. Downstream of the PI, the CVI sampling system was operated to measure residual particle concentration ( $N_{\text{res}}$ ) and condensed water content (CWC) of liquid or frozen hydrometeors passing the PI. In the laboratory it was not possible to exactly simulate the field sampling conditions for the PI. In the field all PI surfaces are exposed to ambient temperatures below  $0^\circ\text{C}$ . In the laboratory only the PI impaction plates were

TABLE 1  
Information about the cloud events presented in this study.

Cloud event	Time period dd.mm. hh:mm–dd.mm. hh:mm	Duration hh:mm	ICE-CVI setup	Temperature °C	Wind speed m/sec	Wind direction
E-1a	02.03. 09:15–02.03. 12:15	03:00	Ice-CVI <sub>(0)</sub>	−16.8 (−17.5,−15.4)	3.5 (0.9,6.2)	WNW (WNW,NW)
E-1b	02.03. 18:40–02.03. 21:30	02:50	Ice-CVI <sub>(2)</sub>	−15.3 (−16.4,−14.4)	4.0 (0.7,6.5)	WNW (WNW,NW)
E-2a	05.03. 06:00–05.03. 09:30	03:30	Ice-CVI <sub>(2)</sub>	−7.3 (−8.9,−3.9)	8.6 (7.4,9.6)	NW (NW,NNW)
E-2b	05.03. 12:10–05.03. 15:20	03:10	Ice-CVI <sub>(0)</sub>	−9.3 (−10.5,−8.4)	3.6 (2.9,4.2)	NW (WNW,NW)
E-3	06.03. 11:30–06.03. 13:00	01:30	Ice-CVI <sub>(1)</sub>	−10.7 (−11.8,−9.6)	5.6 (4.8,6.6)	NW (WNW,NNW)
E-4	22.03. 16:00–22.03. 16:30	02:30	Ice-CVI <sub>(1)</sub>	−15.8 (−16.7,−13.6)	1.1 (0.2,4.6)	NW (WNW,NW)
E-4	22.03. 17:30–22.03. 18:30					
E-4	22.03. 20:30–22.03. 21:30					
E-5	23.03. 00:30–23.03. 03:00	02:30	Ice-CVI <sub>(1)</sub>	−17.0 (−17.5,−16.5)	2.3 (0.3,4.8)	NW (WNW,NW)
E-6	23.03. 19:15–23.03. 21:00	10:45	Ice-CVI <sub>(1)</sub>	−17.5 (−18.3,−15.8)	5.2 (1.1,10.9)	WNW (WNW,NW)
E-6	24.03. 00:00–24.03. 09:00					
E-7	24.03. 14:00–24.03. 24:00	10:00	Ice-CVI <sub>(3)</sub>	−17.4 (−18.7,−15.8)	2.1 (0.1,4.4)	WNW (WNW,NNW)
E-8	27.03. 03:10–27.03. 08:10	05:00	Ice-CVI <sub>(0)</sub>	−17.2 (−18.3,−15.3)	7.7 (4.5,10.5)	SE (ESE,SSE)
E-9	30.03. 17:20–30.03. 22:50	05:30	Ice-CVI <sub>(0)</sub>	−10.6 (−12.1,−8.1)	13.5 (11.5,16.7)	SE (ESE,SSE)
E-10	01.04. 15:30–02.04. 01:30	10:00	Ice-CVI <sub>(0)</sub>	−8.3 (−10.5,−5.1)	7.8 (11.5,16.7)	SSE (SE,WSW)
E-11	03.04. 07:40–03.04. 17:40	10:00	Ice-CVI <sub>(0)</sub>	−5.9 (−8.9,−2.5)	4.7 (0.2,7.6)	SE (ESE,NNW)

Mean meteorological parameters are provided by the Swiss national weather service MeteoSwiss for the Jungfrauoch station (min. and max. of 10-minute averages are given in parentheses).

cooled down to  $-5$  and  $-20^{\circ}\text{C}$  in order to study the freezing and bouncing off of the impacting liquid drops and ice particles, respectively. In PI test runs with liquid drops, no residual particles and no condensed water was detected, e.g., no drops larger than the lower CVI cut size of  $5\ \mu\text{m}$  left the PI. Since control runs without the PI confirmed that drops larger than  $5\ \mu\text{m}$  were present it is concluded that the pre-segregation efficiency of the PI for liquid drops larger than  $5\ \mu\text{m}$  is 1.

When the drops were frozen before entering the PI, residuals and condensed water were observed by the CPC and the hygrometer downstream of the CVI. No changes in the measured parameters could be seen when the impaction plate surfaces were dry or already covered by frozen water from impacted supercooled drops. Thus it is excluded that the ice particles produce secondary ice particles larger than  $5\ \mu\text{m}$  when they hit the frozen water on the plates. The occurrence of other secondary particles (ice particle shattering and abrasion of stainless steel particles) has already been ruled out due to the low air velocity in the PI. In combination with the fact that ice particles readily bounce off from ungreased plates (Murphy et al. 2004) a high PI transmission efficiency for ice particles is expected. This assumption will be further evaluated in the discussion of the field measurements.

## 4. FIELD EXPERIMENT

### 4.1. Location of the Sampling Site

The Ice-CVI was deployed at the high alpine research station Jungfrauoch (JFJ, 3580 m asl,  $46^{\circ}33'\text{N}$ ,  $7^{\circ}59'\text{E}$ ) within

the framework of the international Cloud and Aerosol Characterization Experiment, CLACE-3, conducted from the end of February to the beginning of April 2004. Long-term aerosol measurements have shown that the JFJ can be regarded as representative for the continental lower free troposphere with only a minor boundary layer air influence in winter (Baltensperger et al. 1997). In winter, the site is frequently wrapped in clouds at temperatures down to  $-30^{\circ}\text{C}$ . Thus, the JFJ is well suited for studies of mixed-phase clouds in the lower troposphere (Henning et al. 2004). Details about the cloud events presented in this study are given in Table 1, including mean temperature, wind velocity and direction measured by MeteoSwiss, the Swiss national weather service.

### 4.2. Ice-CVI Setup

The vertical Ice-CVI inlet system was mounted on a platform above the Sphinx laboratory with a distance of 2 m between the omni-directional inlet and the surface. On the platform no wind measurements were available. Later tests showed that the wind velocity at the platform was significantly lower than the simultaneous MeteoSwiss values (especially for wind directions between WNW and NNW) measured at another location of the Sphinx Observatory. Thus, the values given in Table 1 should be considered as upper limits of the wind velocities at the Ice-CVI inlet.

All sensors for the residual particle analysis were located in the Sphinx laboratory directly beneath the platform. In parallel to the standard devices (CPC, PSAP, Lyman- $\alpha$  hygrometer) further instrumentation was coupled to the Ice-CVI (Figure 3).The

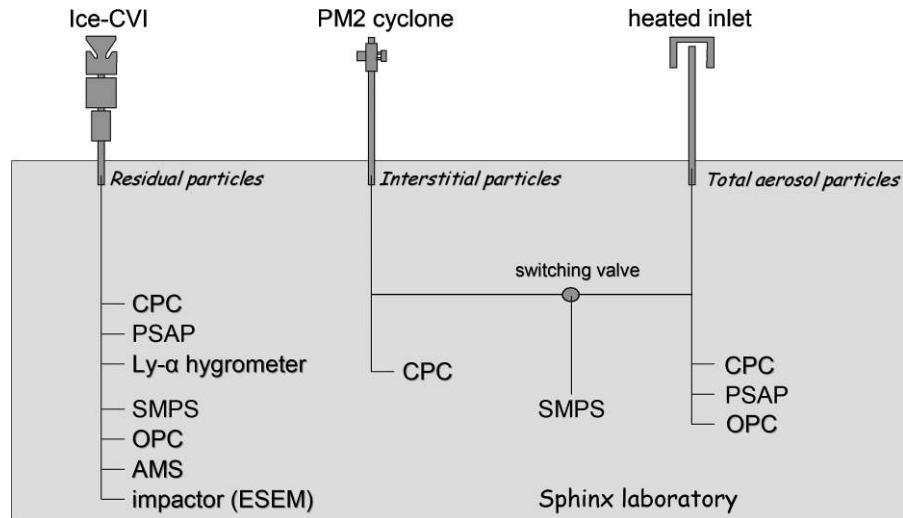


FIG. 3. Schematic drawing of all inlets on the platform and connected instrumentation located beneath inside the Sphinx laboratory. One SMPS was operated at the total and interstitial inlet by means of a switching valve.

particle number size distribution was measured with a Scanning Mobility Particle Sizer (SMPS,  $20 \text{ nm} < d_p < 800 \text{ nm}$ ) and an Optical Particle Counter (OPC,  $0.3 \text{ }\mu\text{m} < d_p < 20 \text{ }\mu\text{m}$ ), where  $d_p$  denotes the dry particle diameter. An Aerodyne Aerosol Mass Spectrometer (AMS,  $20 \text{ nm} < d_p < 1 \text{ }\mu\text{m}$ , Jayne et al. 2000; Schneider et al. 2006) was used to determine total mass concentration and mass size distributions of sulfate, nitrate, ammonium, and organic matter (OM). The aerosol particles are vaporized inside the AMS at a surface heated to  $600^\circ\text{C}$ . Hence all substances with a higher vaporization temperature cannot be detected. Moreover, aerosol samples were collected by a two stage impactor for off-line analysis with the Environmental Scanning Electron Microscope (ESEM, Ebert et al. 2002) in order to derive the morphology and elemental composition of single residual particles. Because all the sampling was carried out at temperatures below  $-5^\circ\text{C}$ , the impaction plates of the PI were not actively cooled, i.e., they adopted the ambient temperature.

#### 4.3. Further Aerosol Inlets

A total and an interstitial aerosol inlet were operated in parallel to the Ice-CVI (Figure 3) within a distance of 1.6 m and a similar inlet height above the Sphinx roof. The total aerosol inlet is heated to  $25^\circ\text{C}$  in order to evaporate/sublimate hydrometeors during sampling as early as possible to avoid transmission losses. This inlet is designed to collect hydrometeors with diameters smaller than  $40 \text{ }\mu\text{m}$  up to a wind speed of  $20 \text{ m s}^{-1}$  (Weingartner et al. 1999). Thus it is possible to sample the entire dried aerosol size distribution inside clouds. The interstitial inlet segregates hydrometeors by a cyclone with a  $2 \text{ }\mu\text{m}$  cut-off. It collects only the small non-activated particles inside clouds. Because the interstitial inlet was not heated clogging by snow and riming was possible. Therefore, it was continuously cleaned, which substantially reduces the occurrence of inlet blocking. The

few remaining periods where clogging occurred have been identified by a pressure drop measured at the interstitial inlet, and are excluded from analysis. Downstream of both inlets, a similar set of instruments as on the Ice-CVI was connected (CPC, PSAP, SMPS, and OPC results will be shown in this study) to simultaneously measure the same parameters of the total and interstitial particle population (Figure 3). Under cloudless conditions the Ice-CVI inlet was operated as an aerosol inlet by switching off the counterflow, whereby all three inlets sample the same ambient aerosol. These periods were used to intercompare all sensors measuring the same parameter on the different inlets.

#### 4.4. Cloud Microphysical Probes

A Particle Volume Monitor (PVM; Gerber 1991) measured the liquid water content (LWC). Its signal is only qualitatively used in this study, because it is not clear to what extent the PVM response is affected by the presence of ice particles. Images of cloud particles larger than  $5 \text{ }\mu\text{m}$  were taken by the Cloud Particle Imager (CPI; Lawson et al. 2001) located on a separate platform 8 m apart and 2 m beneath the Ice-CVI installation. From this information, number size distributions of differently shaped hydrometeors are obtained up to ice particle sizes of  $2500 \text{ }\mu\text{m}$ . The CPI analysis is carried out according to Connolly et al. (2007) where the determination of ice particle concentration is significantly improved (by experimentally determining the size-dependent depth of field of the CPI) and the oversizing of ice particles is corrected. Both issues substantially increase the CPI sensitivity for small hydrometeors. All non-spherical particle shapes can be assigned to ice particles whereas the habit type “spherical” could contain liquid and recently frozen drops. The CPI analysis also allows one to infer the IWC for different habit types or for different size classes by means of shape and size

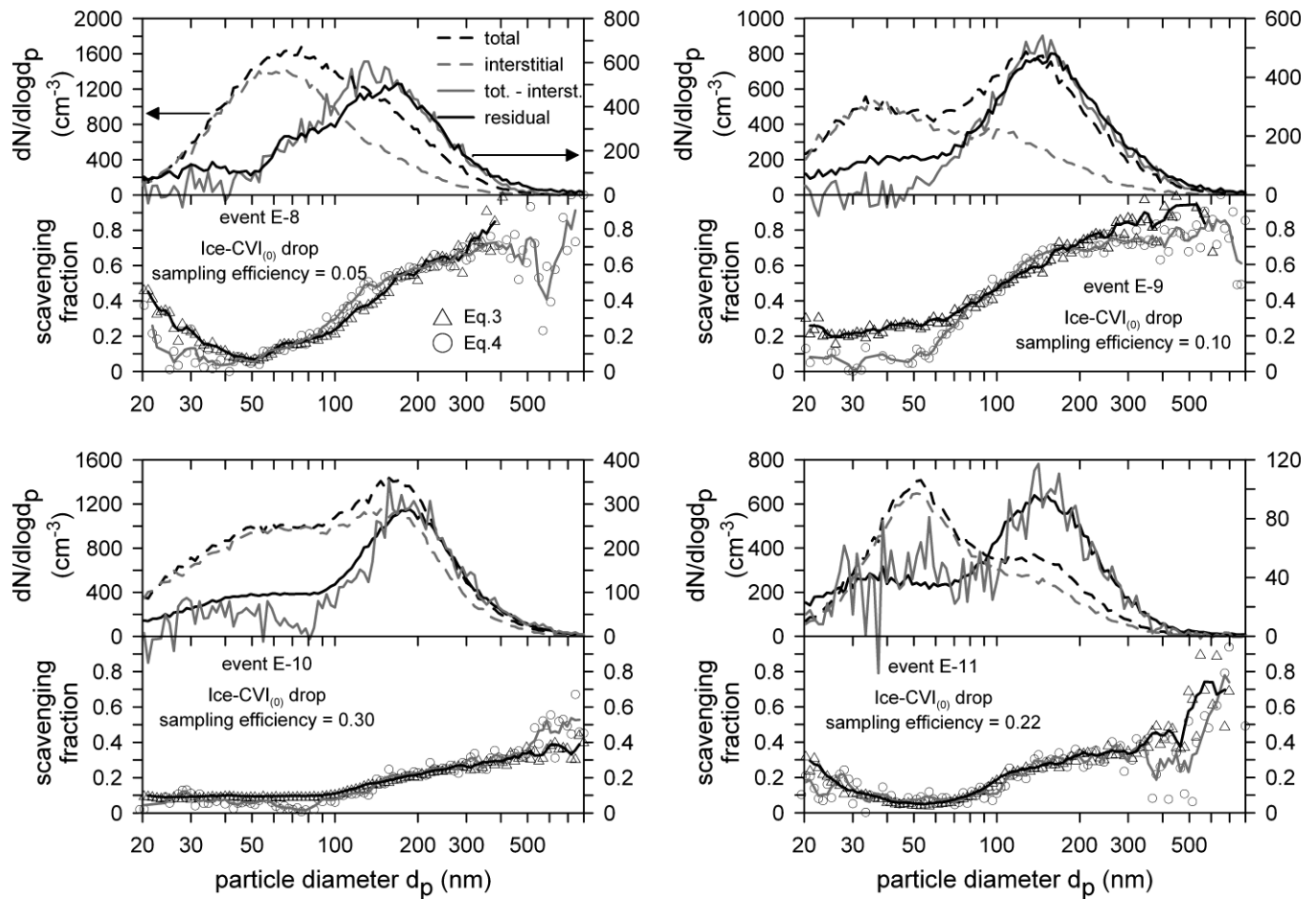


FIG. 4. Comparison of particle number size distributions when drops were present and neither VI nor PI was installed in the Ice-CVI setup. Upper panels: mean number size distributions of total (dashed black), interstitial (dashed grey) and residual (solid black, right scale) particles and (total—interstitial) (solid grey, right scale). Lower panels: Scavenging fractions derived from Equation (3) (open triangles, black line) and Equation (4) (open circles, grey line) as a function of particle diameter. Cloud event and the Ice-CVI<sub>(0)</sub> sampling efficiency for supercooled drops are indicated.

dependent parameterizations of the ice particle mass (Heymsfield et al. 2004).

Due to the low wind speeds on the ground-based platform compared to aircraft measurements, droplet and/or crystal shattering at the CPI instrument was minimal. Significant shattering, which could be identified by the CPI-measured ice particle shapes, occurred only during heavy precipitation periods. This was not the case for CPI data presented here.

## 5. RESULTS

### 5.1. Ice-CVI Setup Without VI and PI (Ice-CVI<sub>(0)</sub>)

The modular design of the Ice-CVI inlet system allows the replacement of the VI or PI or both by cylindrical tubes having a diameter of 4 cm. An Ice-CVI configuration without any pre-impactor (Ice-CVI<sub>(0)</sub>) was temporarily deployed, because only this setup allows the comparison of the Ice-CVI sampling to the difference of total and interstitial inlet aerosol collection. This implies the simultaneous sampling of small ice particles and

supercooled drops under mixed-phase conditions but without a sharp upper cut size and with the possibility of contamination by precipitating and windblown particles. Four measurement examples of the total, interstitial (black and grey dashed lines, upper panels, left scale) and residual particle (black solid line, upper panels, right scale) mean number size distributions are shown in Figure 4. Additionally, the difference of total and interstitial number size distribution (TOT-INT, grey solid line, right scale) is plotted. In the lower panels the size resolved scavenging fraction  $F_N(d_p)$  is shown which is calculated in two different ways by Equation (3) (open triangles) and Equation (4) (open circles).

$$F_{N,\text{res}}(d_p) = \frac{\frac{dN_{\text{res}}(d_p)}{d \log d_p}}{\frac{dN_{\text{tot}}(d_p)}{d \log d_p}} \quad [3]$$

$$F_{N,\text{tot-int}}(d_p) = \frac{\frac{dN_{\text{tot}}(d_p)}{d \log d_p} - \frac{dN_{\text{int}}(d_p)}{d \log d_p}}{\frac{dN_{\text{tot}}(d_p)}{d \log d_p}} \quad [4]$$

Here,  $N_{\text{tot}}$  and  $N_{\text{int}}$  are the number concentration of total and interstitial aerosol particles, respectively.  $F_N(d_p)$  denotes the fraction of activated particles as a function of particle size. When supercooled drops are present they usually dominate the ice particles in terms of number, so that the residual and TOT-INT number size distribution and  $F_N(d_p)$  should be almost completely ascribed to drop residual particles that served as cloud condensation nuclei (CCN). Indeed, the residual particle number size distribution measured with the CVI without VI and PI agrees qualitatively very well with the difference of total and interstitial number size distribution for all events. However, the Ice-CVI<sub>(0)</sub> measurements had to be scaled to achieve a good quantitative agreement for the CCN mode above 100 nm, which simultaneously causes the consistency of the differently derived  $F_N(d_p)$  curves. From this scaling factors a sampling efficiency for supercooled drops was inferred for each cloud event which is in the range of 5–30% (cf. Figure 4). It is supposed that the high wind speeds at south easterly winds (cf. Table 1), leading to a significantly reduced aspiration efficiency of the omni-directional inlet (Figure 1), in combination with drop freezing on the walls of the long tubes that replace VI and PI in front of the CVI tip, are responsible for the low drop collection efficiencies during the presented cloud events.

In warm clouds  $F_N(d_p)$  usually shows a rather steep increase from 0 to 1 in the region of the 50% activation diameter (Mertes et al. 2005). From Figure 4 it is obvious that  $F_N(d_p)$  is diverse under mixed-phase conditions (esp. during cloud event E-10 and E-11). This deviation has been attributed to drop evaporation caused by the Bergeron-Findeisen process (Henning et al. 2004; Schwarzenböck et al. 2001) and is discussed in detail for the CLACE-3 measurements by Verheggen et al. (2007).

Another feature seen in the TOT-INT as well as in the residual number size distributions (Figure 4) is the existence of particles in the size range between 20 and 50 nm. Residual particles in this size range originating from drops in warm clouds have been observed before (Schwarzenböck et al. 2000). They were explained by highly soluble CCN material and high supersaturations (1% or more) occurring through the orographic effect of a mountain site. However, the scavenging fraction at this diameter range was about 0.05 and decreased for smaller sizes, whereas in the actual study  $F_N(d_p)$  reaches values between 0.1 and 0.2 and sometimes increases for smaller diameters. A sampling artifact of the Ice-CVI<sub>(0)</sub> is unlikely, because the same characteristic is found for the TOT-INT number size distribution. It might be possible that these small residues are related to the collection of ice particles by both the CVI and the total inlet. This hypothesis will be addressed in section 5.5. Since the sampling efficiency of the Ice-CVI<sub>(0)</sub> system for ice particles should be higher than for supercooled drops (due to bounce off instead of freezing at the tube walls), the aforementioned up-scaling of the residual particle size distribution might be too large in the particle size range below 50 nm. This suggestion is supported by the fact that the residual particle size distributions in Figure 4 are systemati-

cally higher than the difference of total and interstitial particles in this size range.

## 5.2. Ice-CVI Setup Including PI but Without VI (Ice-CVI<sub>(1)</sub>)

In this section the impact of the PI on the Ice-CVI sampling characteristics under mixed-phase conditions is studied. In order to examine the pre-segregation of supercooled drops by the PI we concentrate on non or only slightly precipitating cloud events at low and moderate wind velocities (i.e., even less influence of blowing snow) where a CCN mode was observed in the TOT-INT number size distribution and where the VI was not installed. Figure 5 shows four cloud events where the CCN mode is visible (solid grey lines in the upper panels, more pronounced in the lower two examples) with a maximum between 150 and 200 nm similar to the respective plots in Fig.4. This time the residual particle number size distribution (solid black lines, upper panels) did not follow the shape of this mode. This is a clear indication that the liquid drops did not pass the PI in contrast to the measurements presented in Figure 4 where the PI was not installed. The residual particle size distributions that are now associated with the collection of ice particles only do not possess a distinct shape but slightly increase to smaller sizes.

Since the TOT-INT number size distribution is composed of residuals from liquid drops and ice particles whereas the Ice-CVI residual number size distribution comprises ice particle residuals only, the condition  $F_{N,\text{res}}(d_p) \leq F_{N,\text{tot-int}}(d_p)$  should be met in the lower panel graphs of Figure 5 over the entire particle diameter range. This constraint is only achieved when calculating the residual size distributions and the resultant scavenging fractions (open diamonds, lower panels) in Figure 5 with an assumed Ice-CVI<sub>(1)</sub> sampling efficiency of about 1. Due to the fluctuations of the TOT-INT number size distribution at the small and large diameter edge (caused by subtraction of two similar numbers and low counting statistics) it is impossible to infer an Ice-CVI<sub>(1)</sub> sampling efficiency for ice particles more precisely.

## 5.3. Ice-CVI Setup Including VI but Without PI (Ice-CVI<sub>(2)</sub>)

The segregation capability of the VI is exemplarily demonstrated in Figure 6. The VI was installed and de-installed during two different cloud events at rather constant meteorological conditions (temperature, wind speed and direction) and continuous precipitation which might include windblown snow. Furthermore, the quite constant signals of total and interstitial particle concentration (Figure 6b, black and grey lines) and in-situ measured LWC (Figure 6d, grey line) imply constant cloud microphysical conditions throughout the selected periods. It is obvious from Figure 6 that the installation of the VI strongly reduces  $N_{\text{res}}$  from several tens to below  $5 \text{ cm}^{-3}$  and the sampled CWC from several hundreds to below  $20 \text{ mg m}^{-3}$ . The effect of using the VI

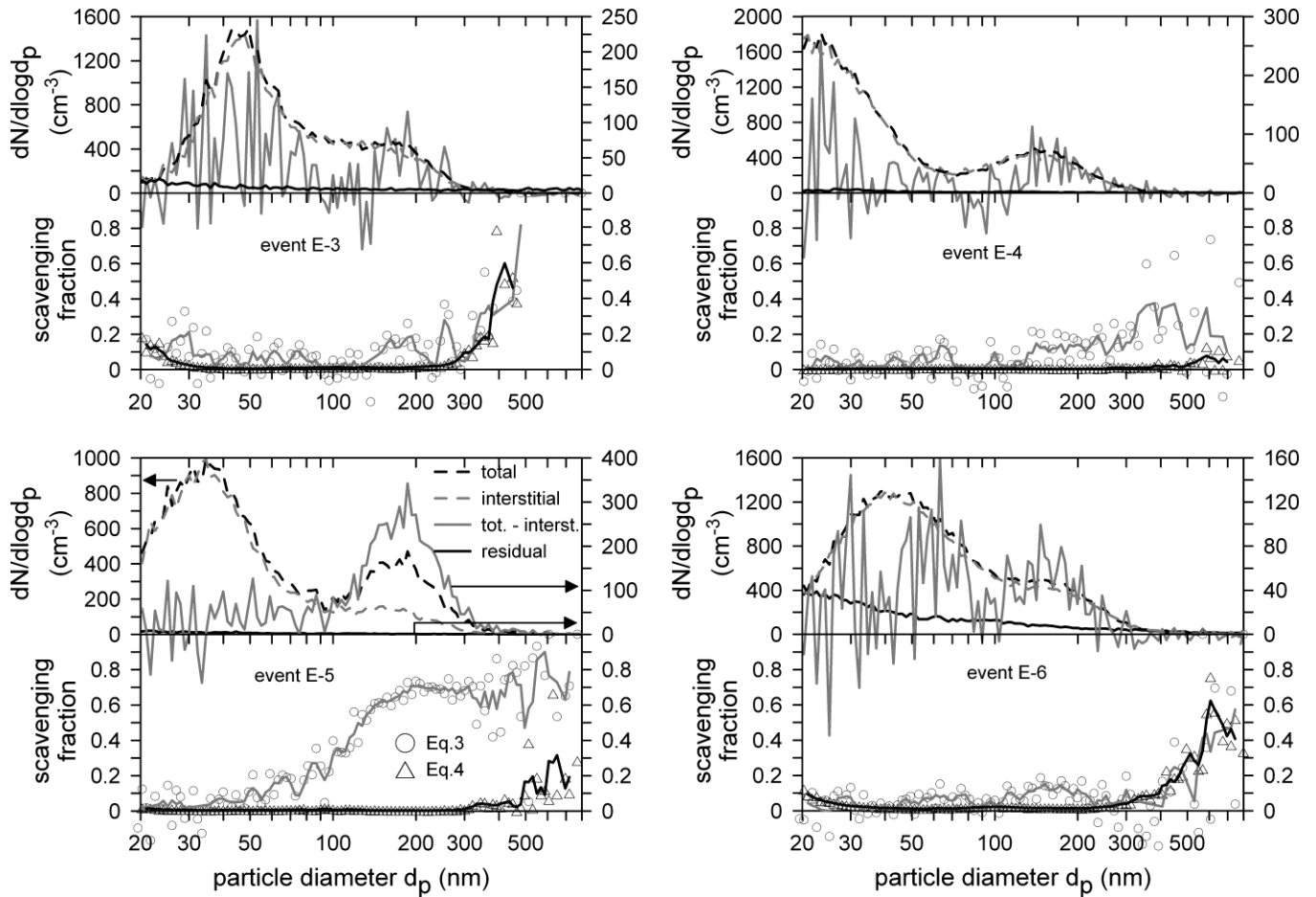


FIG. 5. Same as Figure 4, but with the PI installed in the Ice-CVI setup to pre-segregate supercooled drops. The Ice-CVI<sub>(1)</sub> sampling efficiency for ice particles is assumed to be unity.

is most clearly seen when looking at the time series of the mean volume diameter of the sampled hydrometeors,  $D_V$ , calculated from Equation (5) and shown in Figure 6e,

$$D_V = \left( \frac{6 \cdot \text{CWC}}{\pi \cdot \rho_{\text{hydro}} \cdot N_{\text{res}}} \right)^{\frac{1}{3}} \quad [5]$$

where  $\rho_{\text{hydro}}$  denotes the density of the hydrometeors and CWC is here the cloud water content sampled by the Ice-CVI. A value of  $0.91 \text{ g cm}^{-3}$  was chosen for  $\rho_{\text{hydro}}$  which represents the solid ice density and is used for small, compact ice particles (Heymsfield et al. 2004). During event E-2a where the VI was installed, the  $D_V$  values were below the upper size limit of  $20 \mu\text{m}$  (Figure 6e) given by the VI (and above the lower limit of  $5 \mu\text{m}$  given by the CVI), whereas without the VI,  $D_V$  was mostly above this limit reaching values of  $40 \mu\text{m}$ . This implies that the higher residual particle concentration and sampled CWC are caused by large ice aggregates that reach the CVI inlet, because they are not pre-segregated by the VI. These agglomerates release several aerosol particles that they have incorporated in

the cloud (due to riming and aerosol scavenging) when they become evaporated inside the sampling system, which artificially reduces  $D_V$  according to Equation (5) to the inferred range of  $40 \mu\text{m}$ . Most likely these are precipitating particles (i.e., larger than  $1 \text{ mm}$ ) that do not follow the stream lines at all but could have trajectories depending on the prevailing wind conditions to infrequently reach and pass the omni-directional inlet. A rough estimation assuming spherical ice aggregates with a diameter of  $5 \text{ mm}$  yields a number concentration of only  $6 \cdot 10^{-3}$  particles  $\text{liter}^{-1}$  to be sufficient to explain the average measured CWC of  $0.4 \text{ g m}^{-3}$  when the VI was not installed. This confirms the very low but still non-zero passing efficiency of the omni-directional inlet for large ice aggregates and the necessity to operate the VI, since already very few collected large particles would cause a large contamination regarding residual number and CWC.

By the way, during the event E-1b the CWC was below the detection limit of the dew point mirror and no Lyman- $\alpha$  hygrometer (which is able to measure CWC below  $10 \text{ mg m}^{-3}$ ) was operated. Thus reasonable  $D_V$  values for this period could not be calculated.

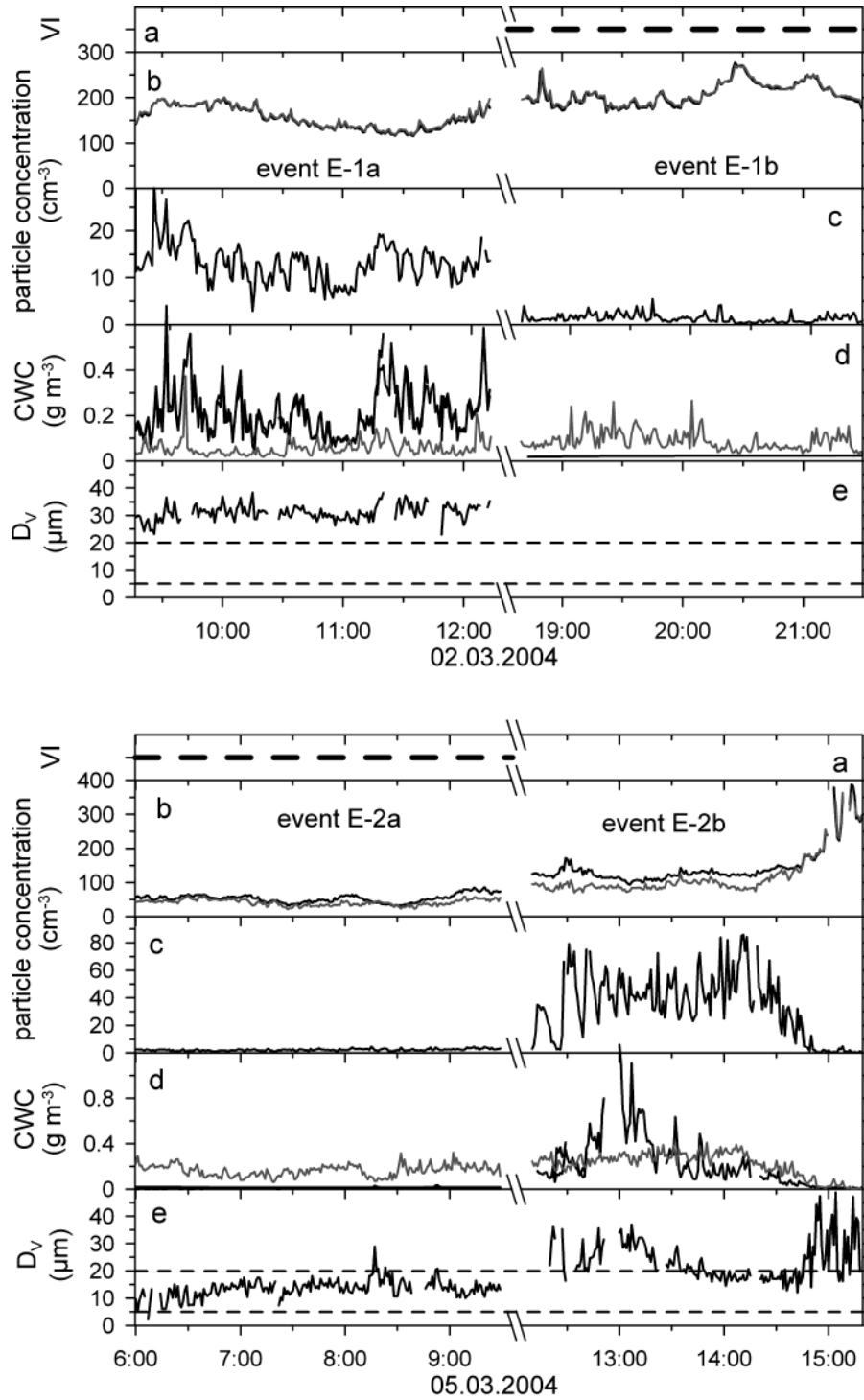


FIG. 6. Time series of total, interstitial and residual particle concentration, condensed water content and mean volume hydrometeor diameter for two different cloud events where the virtual impactor (VI) was installed (thick dashed line)/de-installed as indicated. (a) VI installed (thick dashed line); (b) total (black line) and interstitial (grey line) particle concentration; (c) residual particle concentration; (d) CWC sampled by the Ice-CVI (black line) and in-situ LWC (PVM, grey line); (e)  $D_v$  of hydrometeors sampled by the Ice-CVI according to Equation (5). Thin dashed lines indicate the intended sampling size range determined by VI (upper limit) and CVI (lower limit).

#### 5.4. Ice-CVI Setup Including VI and PI (Ice-CVI<sub>(3)</sub>)

The findings presented in the previous sections imply that the Ice-CVI operated in a complete setup (VI and PI installed in front of the CVI) only collects small ice particles. For one sampling period of 10 hours (event E-7) the complete Ice-CVI setup was operated under rather constant meteorological and cloud microphysical conditions. Time series of different parameters during this event are shown in Figure 7. In the middle and lower panel, IWC and residual particle concentration ( $N_{\text{res}}$ ) sampled with the Ice-CVI<sub>(3)</sub> is compared to IWC and ice particle concentration ( $N_{\text{ice}}$ ) time series derived from in-situ measurements by means of the CPI. The CPI provides size resolved concentra-

tions of differently shaped hydrometeors with a size bin width of  $10 \mu\text{m}$ . In order to compare the Ice-CVI<sub>(3)</sub> measurements to the CPI results, only the first two CPI size bins ( $5\text{--}15 \mu\text{m}$  and  $15\text{--}25 \mu\text{m}$ ) are used to calculate the ice particle concentration  $N_{\text{ice}}$  and IWC. However, it should be kept in mind that the CPI counting efficiency for particles smaller than  $10 \mu\text{m}$  is underdetermined and is difficult to correct for owing to the discrete nature of the CPI images ( $10 \mu\text{m}$  represents 4 pixels across on the image). The counting efficiency of the next size bin is quantitative due to the CPI data analysis carried out according to Connolly et al. (2007). Besides, the upper size bin limit of  $25 \mu\text{m}$  is somewhat larger than the Ice-CVI cut size.

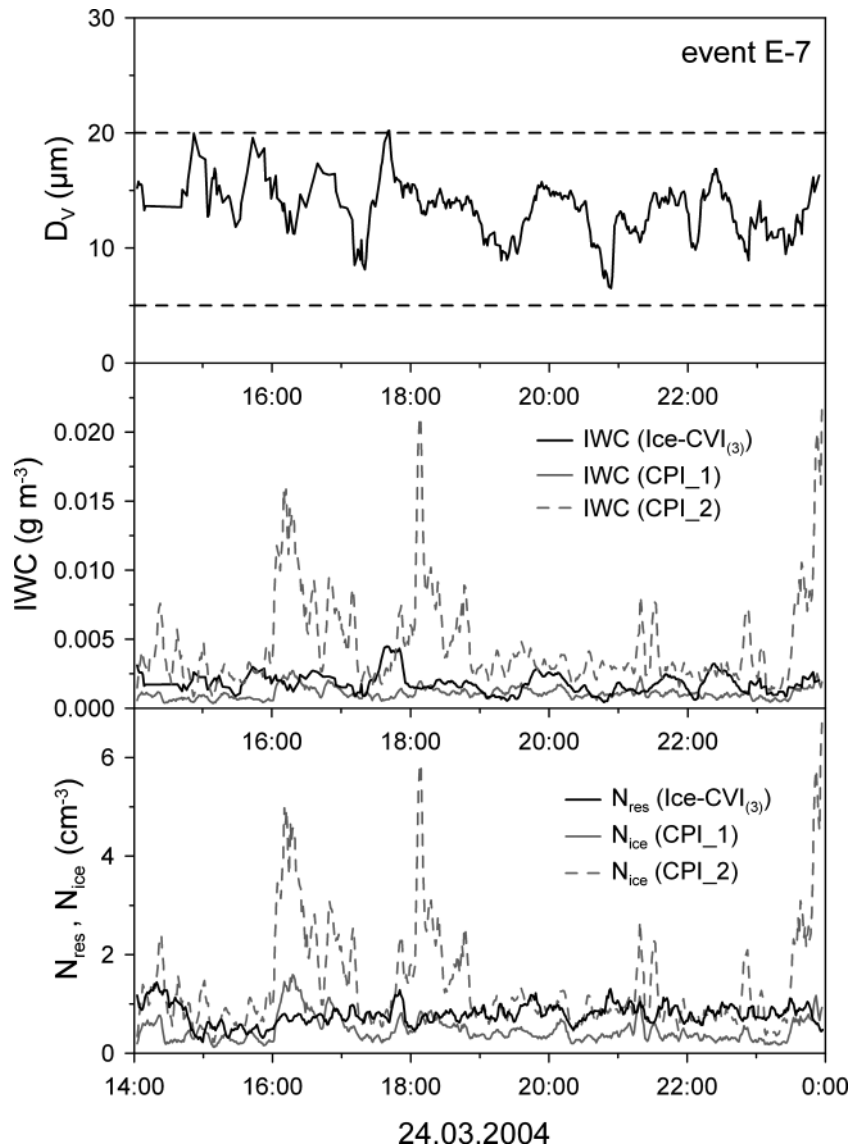


FIG. 7. Middle and lower panel: Time series during event E-7 of IWC and  $N_{\text{res}}$  from small ice particles sampled by the Ice-CVI<sub>(3)</sub> (solid black line). Grey lines indicate CPI measurements of IWC and  $N_{\text{ice}}$  in the size range from  $5$  to  $25 \mu\text{m}$ , completely ignoring spheroids (CPI1, solid lines) and including spheroids of the larger size bin (CPI2, dashed lines). Upper panel: Time series of  $D_V$  (Equation [5]) (solid line) and lower and upper cut size limits of  $5$  and  $20 \mu\text{m}$  (dashed horizontal lines) of the Ice-CVI<sub>(3)</sub> setup.

Only four particle habits as classified by the CPI analysis software are found in the 5–25  $\mu\text{m}$  size range: spheroid, small irregular, columnar and stellar, where the latter two had a negligible abundance. The spheroid habit is expected to represent liquid drops but it might contain a number of frozen drops that are still almost spherical. Therefore, it is not clear whether IWC (again using a bulk ice density of  $0.91\text{ g cm}^{-3}$ ) and  $N_{\text{ice}}$  should be inferred by totally or partially ignoring spherical hydrometeors. Thus, two different IWC and  $N_{\text{ice}}$  time series are calculated from the CPI measurements and shown in Figure 7. The solid grey lines disregard all spheroids (CPL1) whereas the dashed grey curves include spheroids of the larger size bin (CPL2). The latter is chosen for two reasons. Due to the Bergeron-Findeisen process the liquid drops should shrink under mixed-phase conditions, i.e., spheroids in the smaller size bin might be most likely still liquid and spheroids in the larger size bin have a higher probability to be frozen. Moreover, larger drops freeze more easily in comparison to smaller ones, at least in the immersion freezing mode (Diehl et al. 2006). Referring to the IWC and particle number comparison it is obvious that IWC and  $N_{\text{res}}$  sampled by the Ice-CVI<sub>(3)</sub> (solid black line) agree well with IWC (CPL1) and  $N_{\text{ice}}$  (CPL1), although both Ice-CVI<sub>(3)</sub> parameters have a tendency to be slightly higher. This is most likely a consequence of the reduced counting efficiency of the CPI in this diameter range. Ice particle shattering inside the PI can be ruled out, because this would only increase  $N_{\text{res}}$  but not the sampled IWC. Average values are  $1.1\text{ mg m}^{-3}$  and  $0.47\text{ cm}^{-3}$  for IWC (CPL1) and  $N_{\text{ice}}$  (CPL1) and  $1.2\text{ mg m}^{-3}$  and  $0.78\text{ cm}^{-3}$  for IWC and  $N_{\text{res}}$  obtained from the Ice-CVI<sub>(3)</sub> sampling, respectively. This means both devices agreed within 10 and 40% with respect to

IWC and  $N_{\text{ice}}$  (in the sense of a 1:1 relation to  $N_{\text{res}}$ ). It is remarkable that the Ice-CVI<sub>(3)</sub> results never exceed IWC (CPL2) and  $N_{\text{ice}}$  (CPL2), respectively. This is in agreement with the assumption that some of the larger spheroids are frozen. The CPI detected on average five times more drops (spheroids) in its first size bin so that Ice-CVI<sub>(3)</sub> measurements of IWC and  $N_{\text{res}}$  higher than the IWC (CPL2) and  $N_{\text{ice}}$  (CPL2) would indicate liquid drop sampling which is not observed at any time. Thus, the hypothesis is favored that the few collected spheroids are frozen, which at the same time supports the assumption that most of the spheroids detected by the CPI are liquid.

Regarding the CPI measurements as a “quasi quantitative” reference demonstrates that IWC and  $N_{\text{ice}}$  are recovered by the Ice-CVI<sub>(3)</sub> at very low absolute IWC and  $N_{\text{res}}$  values between  $1\text{--}5\text{ mg m}^{-3}$  and  $0.2\text{--}1.2\text{ cm}^{-3}$  in the presented cloud event. This implies that ice particles between 5 and 20  $\mu\text{m}$  are sampled with a high but not quantifiable sampling efficiency. An independent verification that the Ice-CVI<sub>(3)</sub> sampling is strongly linked to residuals of ice particles in the intended size range is given by the mean volume diameter  $D_V$  (Figure 7, upper panel), which is within the sampling size limits of the Ice-CVI<sub>(3)</sub> during the entire cloud period.

### 5.5. First IN Characterization by Means of the Ice-CVI

The event E-7 is investigated in detail to characterize IN in the lower free troposphere. The averaged sub-micrometer size distribution of the ice particle residuals is shown in Figure 8 (upper panel,  $dN/d\log d_p$  multiplied by 1000) in conjunction with the total particle size distribution. The most striking feature is the increase of the ice particle residual size distribution to small

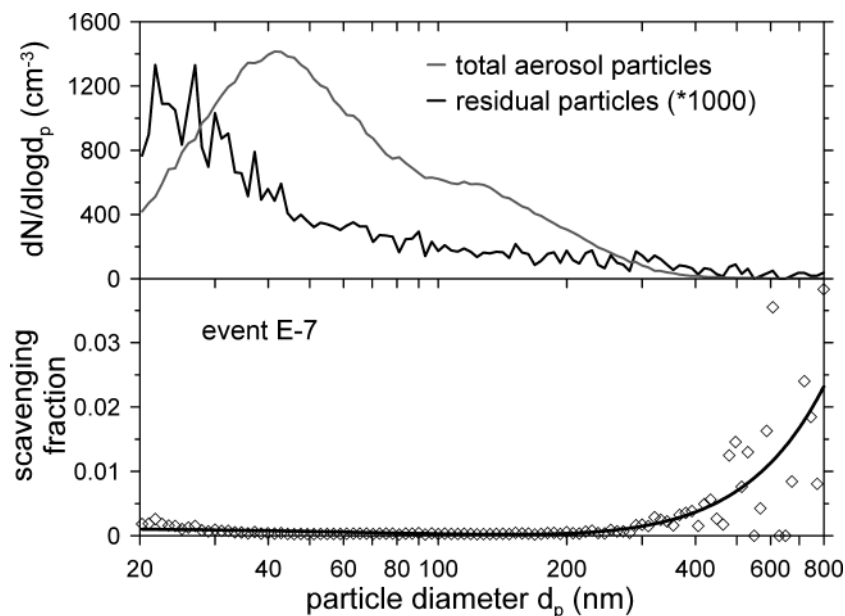


FIG. 8. Upper panel: Mean total (grey curve) and residual (black curve, \*1000) particle number size distributions obtained from SMPS measurements within the same cloud period as results shown in Figure 7 (event E-7). Lower panel: Scavenging fraction derived from Equation (3) as a function of particle diameter (open diamonds).

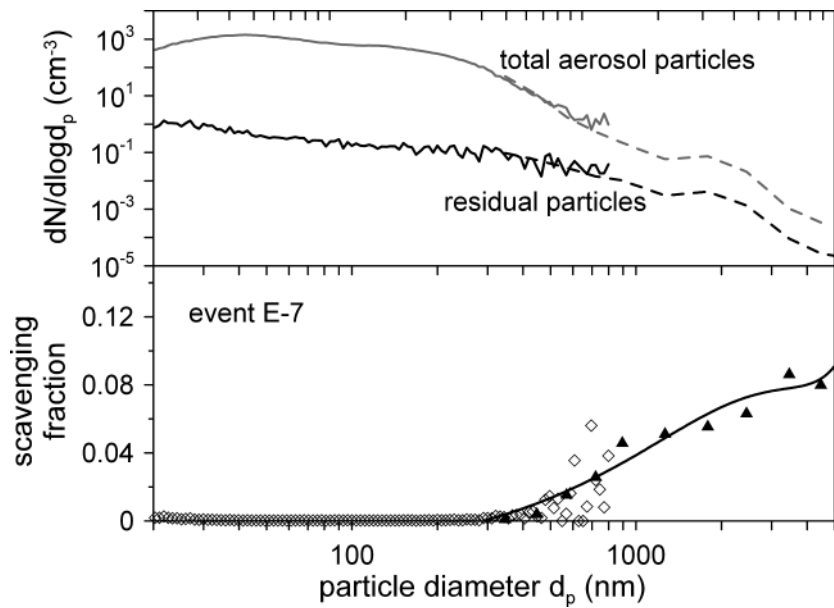


FIG. 9. Same as Figure 8 but size distributions measured by the two OPC (dashed lines) and the resulting scavenging fraction (triangles) are added.

diameters that results in a slight increase of the scavenging fraction (Figure 8, lower panel) below 40 nm. This behavior was also observed in Figures 4 and 5 not only for the Ice-CVI sampling but also for the TOT-INT size distributions implying that the same effect occurred when the ice particles were sampled by the heated total inlet. Due to the good agreement of residual and ice particle concentration demonstrated in the preceding paragraph it can be excluded that the small residuals result from ice particle shattering inside the Ice-CVI system or from particle scavenging by riming or impaction after ice particle formation. However, it is not clear whether the small residual particles acted as IN, because they might originate from condensable matter inside those ice particles, that have been produced by secondary ice formation processes. The existing low temperatures and the absence of small columnar crystals in the first two CPI size bins do not support ice multiplication processes like rime splintering (Hallett-Mossop mechanism) and drop fragmentation during freezing but the mechanical fracturing of falling or windblown ice crystals, especially during snow fall, might be possible (Rogers and Yau 1991).

The main increase of the scavenging fraction (Figure 8, lower panel) is observed at large particle diameters starting above 280 nm and well separated by a minimum at intermediate sizes from the small increase for diameters below 40 nm. Therefore, these residuals are not expected to be linked to secondary ice particles and are regarded as IN demonstrating that large particles are preferred to nucleate ice. This statement is confirmed by extending the investigated diameter range to super-micrometer sizes. In Figure 9 (upper panel) the total and residual particle number size distributions determined simultaneously by the two OPCs connected to the total and Ice-CVI inlet, respectively, are added to the SMPS results. It is noticeable that the residual particle

size distribution decreases less steeply than the size distribution of the total particles (sedimentation losses of super-micrometer particles in the sampling lines have been not accounted for but should be similar for both inlets). Consequently, the scavenging fraction (Figure 9, lower panel) increases from 0.03 at  $d_p = 0.8 \mu\text{m}$  to 0.09 at  $d_p = 5 \mu\text{m}$ . Although the absolute majority of IN were found below  $1 \mu\text{m}$ , only every thousandth sub-micrometer but already every tenth super-micrometer particle acted as IN. This finding is restricted to particle diameters up to  $5 \mu\text{m}$ , since larger non-activated particles could enter the CVI.

It is interesting to note that the black curve in Figure 9 (upper panel) looks very similar in shape and number to residual number size distributions measured from aircraft (Seifert et al. 2003) in pure ice clouds (excluding cirrus) above 6 km and at temperatures below  $-30^\circ\text{C}$ .

The chemical characterization of the ice residuals was carried out in different ways. Mass size distributions of soluble aerosol substances were measured by the AMS. Unfortunately, the AMS was not coupled to the Ice-CVI during event E-7. However, it was measuring downstream of the CVI in a preceding period inside the same cloud (event E-6). The Ice-CVI was operated in an Ice-CVI<sub>(1)</sub> setup, i.e., that supercooled drops were pre-segregated but a contribution by precipitating ice aggregates could not be completely ruled out. In Figure 10 the single and summed up AMS mass distributions are shown simultaneously with the total residual mass concentration distribution derived from the SMPS measurements assuming spherical particles and a dry particle density  $\rho_p$ . For a direct comparison, the SMPS distributions have been converted from the mobility diameter  $d_p$  into a vacuum aerodynamic diameter  $d_{va}$  measured by the AMS using  $d_{va} = \rho_p / \chi d_p$  (Schneider et al. 2006) where  $\chi$  denotes the

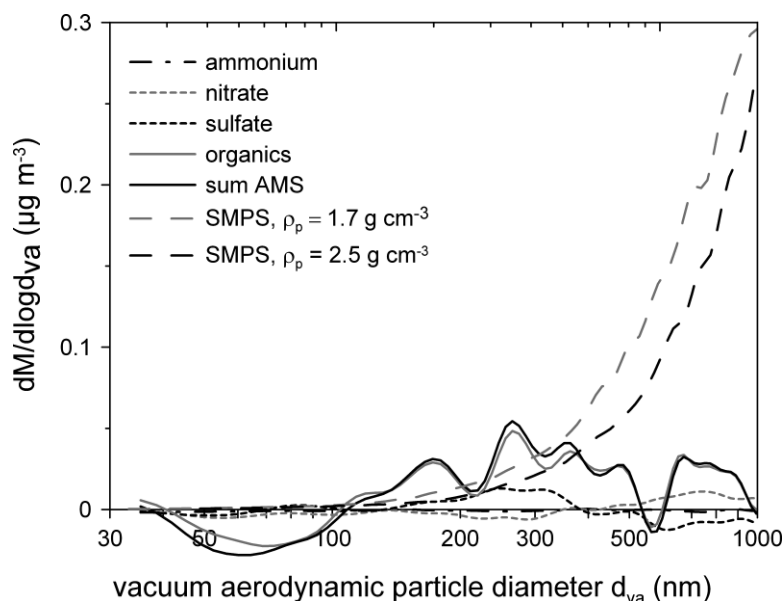


FIG. 10. Mass size distributions of different aerosol compounds (cf. legend) measured with the AMS (Ice-CVI<sub>(1)</sub> setup) and two mass size distributions inferred from the SMPS number size distribution (dashed black and grey line) assuming spherical particles with a density of 1.7 and 2.5 g cm<sup>-3</sup>, respectively. For direct comparison, mass distributions are shown as a function of the vacuum dynamic diameter measured by the AMS.

dynamic shape factor which is assumed to be unity. Two SMPS mass size distributions are shown in Figure 10, which were calculated for a lower and upper limit of  $\rho_p$  with 1.7 and 2.5 g cm<sup>-3</sup>, whereas the latter is a typical value for pure mineral dust particles (Linke et al. 2006). Mass distributions assuming intermediate dry particle densities (e.g., black carbon with  $\rho_p \approx 2$  g cm<sup>-3</sup>) are located in between the two SMPS curves. It is interesting to note that the SMPS distribution assuming the lower  $\rho_p$  is located above the second one indicating that the increase in mass due to a higher density is over-compensated by the shift to a larger  $d_{va}$ . However, both SMPS derived total residual mass distributions begin to increase and to significantly deviate from the residual mass distribution determined by the AMS at  $d_{va}$  values between 400 and 500 nm. It is unlikely that this deviation is caused by aerosol mass entering the Ice-CVI due to precipitating ice aggregates, because the aerosol particles that might be incorporated by riming or impaction scavenging should have the chemical composition of the total aerosol. This population is mainly composed of substances that are observable by the AMS (sulfate, nitrate, ammonium, and volatile organic matter). Therefore we conclude that the missing mass is related to IN that consists of refractory compounds not vaporizable at 600°C and thus not detected with the AMS. Indeed, the mass concentration obtained from the SMPS is well above the detection limit of the AMS (Walter et al. 2006). This means, that if the sampled residual mass had mainly consisted of non-refractory particles it would have been detected by the AMS. The conclusion that refractory substances constitute the IN is also supported by the fact that the deviation of SMPS and AMS residual mass occurs in the same diameter range (in terms of  $d_p$ ) as the increase of the IN

scavenging fraction (Figure 8, lower panel), although it should be considered that both observations were not made at the same time. From Figure 10 it might be additionally suggested that organic matter (OM) is present in the residual particles above  $d_p = 200$  nm accounting for about 15% of the sub-micrometer IN mass. However, this absolute OM fraction should be handled with caution, because the inferred total OM mass of the residual particles is close to the theoretical AMS detection limit.

Further indication of the chemical composition of the sampled IN during E-7 (Ice-CVI<sub>(3)</sub> setup) are obtained from the results of two PSAPs that were connected to the total and Ice-CVI inlet. The PSAP downstream the Ice-CVI was operated with a maximum integration time of 5 min and a high sample flow rate of 4 liter min<sup>-1</sup>. In combination with the CVI enrichment by a factor of 7 a detection limit of about 0.2 ng m<sup>-3</sup> was achieved. Mean BC mass concentrations of 0.7 and 79.1 ng m<sup>-3</sup> were derived for the residual and total aerosol particles, respectively. Since BC is present in the sub-micrometer particles, the BC mass concentrations can be related to the mean residual and total particle mass of 3.9 and 1850 ng m<sup>-3</sup> inferred from the integral over the corresponding SMPS mass distributions (assuming  $\rho_p = 2.5$  g cm<sup>-3</sup>). Fractions can be described in two different ways: First, the fraction of BC mass to SMPS derived mass is 18% for the residual while it is only 4% for the total aerosol reservoir, respectively. Second, 0.9% of the total aerosol BC but only 0.2% of the total aerosol SMPS mass is found in the residuals. Both observations suggest that BC is enriched in the residual particles compared to the totally abundant particles, which implies that BC containing particles may have served as IN inside the examined mixed-phase cloud.

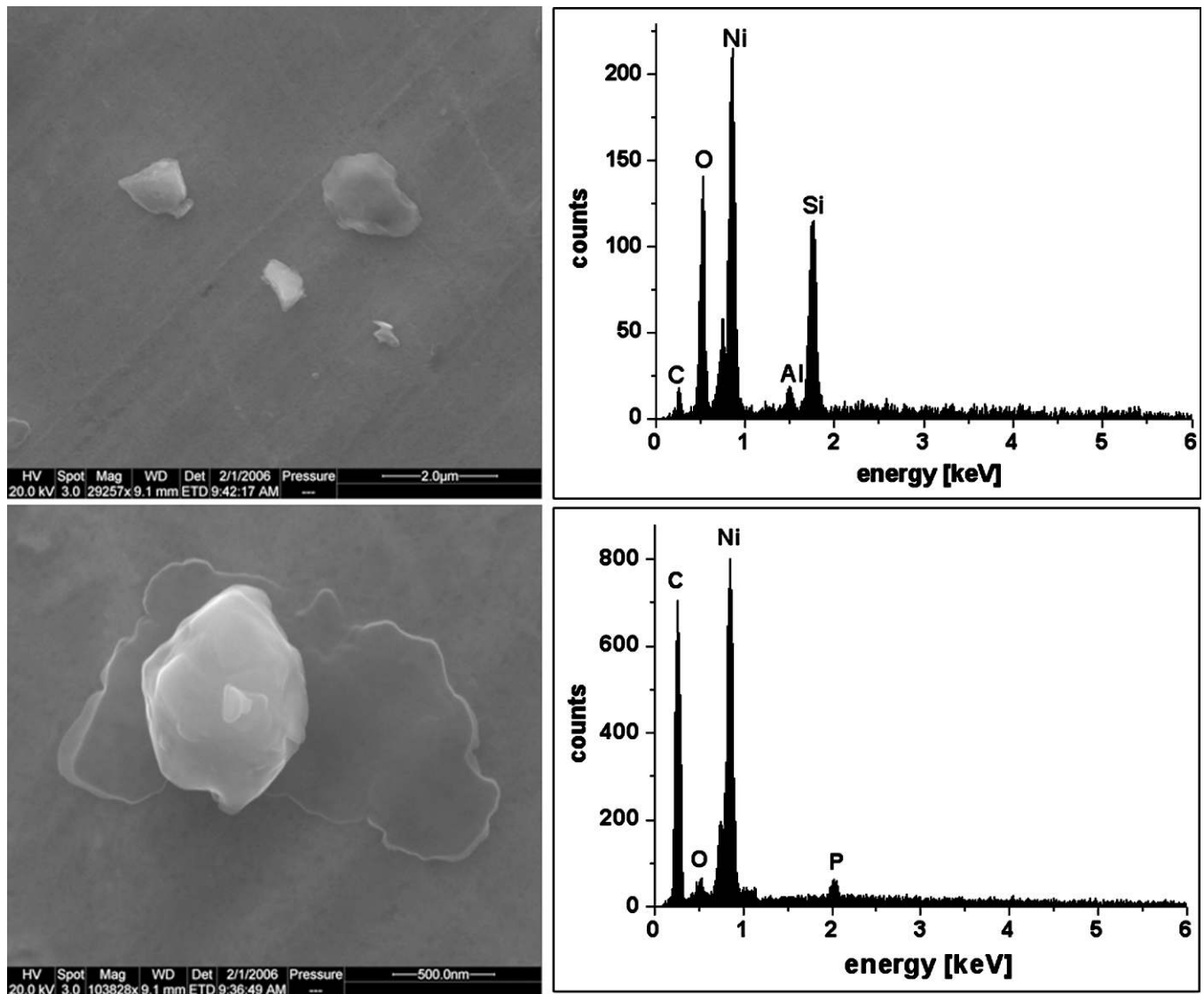


FIG. 11. Secondary electron image and EDX spectrum of residual particles collected with a Ice-CVI<sub>(3)</sub> setup during cloud event E-7. Upper part: super- and sub-micrometer mineral dust (Si) particles (mainly Si). Lower part: sub-micrometer carbonaceous particle. The Ni peak is caused by the substrate.

Nevertheless, only a fraction (about 30%) of the IN mass inferred from the SMPS results could be explained by OM and BC. Moreover the main IN mass is found in the super-micrometer size range according to the OPC number size distribution (Figure 9, upper panel). Assuming again  $\rho_p = 2.5 \text{ g cm}^{-3}$  and a spherical particle shape yields an IN mass of  $11.9 \text{ ng m}^{-3}$  for residual particles above the SMPS size range. Although the assumption of sphericity for super-micrometer particles is not very realistic, this estimation reveals a factor of three more mass in the super-micrometer compared to the sub-micrometer residual particle size range. Hence, the postulated existence of refractory particles derived from the AMS results and the observed existence of an excessive fraction of large particles (in relation to the total aerosol population) in the residual particles leads to the

suggestion that mineral dust particles are a strong candidate for being IN.

Siliceous particles were indeed found as the dominant component in the super-micrometer (19 of 23 analyzed particles) and as an abundant component in the sub-micrometer size range (19 of 125 analyzed particles) by the single particle analysis with ESEM (Figure 11, all four particles in the upper part), which confirms the importance of mineral dust particles as IN in the lower and middle troposphere. This is in agreement with the glaciation of supercooled altocumulus clouds by Saharan dust layers observed by remote sensing techniques (Ansmann et al. 2005; Sassen et al. 2003). In addition, the ESEM analysis (Figure 11, lower part) verifies the dominance of smaller ( $d_p$  mainly between 0.3–1 μm) carbon rich particles (106 of

125 analyzed particles) that are at least non-volatile until 300°C which is consistent with OM and BC found in the residual particles by means of AMS and PSAP. The morphology of the carbon rich particles rules out soot particles as part of the residuals but rather suggests organic particles, which is further supported by the C and O peak in the EDX spectrum shown in Figure 11. The large C and small O signal might imply a contribution of elemental carbon which was most likely seen as BC by the PSAP.

However, Si and C particles are by far the most prominent particle types sampled by the ESEM impactor downstream of the Ice-CVI during event E-7 (Ice-CVI<sub>(3)</sub> setup). From the ESEM analysis, it was additionally verified that no significant contamination by abraded particles (stainless steel, brass, or aluminum) from the Ice-CVI itself could be observed for the Ice-CVI<sub>(3)</sub> setup. This confirms that abrasion does not occur as already argued in section 3 (sampling issues).

## 6. SUMMARY

A novel sampling system, called the Ice-CVI, consisting of different modular components upstream of a counterflow virtual impactor, CVI, was designed to extract small ice particles with diameters between 5 and 20  $\mu\text{m}$  out of mixed-phase clouds by segregating large and precipitating ice aggregates, supercooled drops and interstitial aerosol particles. In a first field experiment the influence of each Ice-CVI component on the sampling behavior of the complete setup was investigated. The omni-directional inlet already restricts the collection of large cloud hydrometeors above the desired diameter range for the most part due to its 90° sampling. Moreover it was shown that the deployment of a virtual impactor, VI, is required to completely discriminate cloud and precipitating particles larger than 20  $\mu\text{m}$ . Downstream of the VI, a pre-impactor, PI, was installed to remove the supercooled drops from the sample volume by freezing the drops on impaction plates. In order to evaluate the drop pre-segregation capability of this impactor, residual particle number size distributions measured downstream of the Ice-CVI were compared to the difference in number size distributions between the total and interstitial particles. It could be demonstrated that an existing CCN mode, which is related to the supercooled drops, disappeared in the residual particles as soon as the PI was installed. This is attributed to a total liquid phase removal inside the pre-impactor which was observed in a lab test with cooled impaction plates. The transmission of the complete Ice-CVI setup for ice particles with  $5 \mu\text{m} < D_{\text{ice}} < 20 \mu\text{m}$  (size limits given by CVI and VI) was tested in a mixed-phase cloud with regard to results obtained by a cloud particle imager, CPI, for a similar ice particle size range. The IWC and particle concentration results of both devices agreed within 10 and 40%, verifying a representative small ice particle collection and thus a representative IN retrieval by the Ice-CVI.

According to the verification of the intended Ice-CVI sampling behavior, the sampled residuals of the mixed-phase cloud

event are analyzed as a first IN characterization case study. Every tenth super-micrometer but only every thousandth sub-micrometer aerosol particle was detected as ice particle residual. This provides evidence that the larger the particle the more it is preferred to act as an IN. However, the sub-micrometer particles dominate the IN number concentration. Mineral dust, non-volatile organic matter, and BC were consistently identified as IN substances by different methods. The latter IN constituents imply an anthropogenic influence on the heterogeneous ice nucleation in tropospheric mixed phase clouds. This might be important because sub-micrometer particles seem to control the ice particle concentration. However, these results are derived from a single mixed-phase cloud and need to be further evaluated by more measurement programs operating the novel Ice-CVI sampling system.

## REFERENCES

- Ansmann, A., Mattis, I., Müller, D., Wandinger, U., Radlach, M., Althausen, D., and Damoah, R. (2005). Ice Formation in Saharan Dust Over Central Europe Observed with Temperature/humidity/aerosol Raman Lidar, *J. Geophys. Res.* 110:doi:10.1029/2004JD005000.
- Baltensperger, U., Gäggeler, H. W., Jost, D. T., Lugauer, M., Schwikowski, M., Weingartner, E., and Seibert, P. (1997). Aerosol Climatology at the High-Alpine Site Jungfraujoch, Switzerland, *J. Geophys. Res.* 102(D16):19707–19715.
- Bond, T. C., Anderson, T. L., and Campbell, D. (1999). Calibration and Inter-comparison of Filter-Based Measurements of Visible Light Absorption by Aerosols, *Aerosol Sci. Technol.* 30:582–600.
- Cantrell, W., and Heymsfield, A. (2005). Production of Ice in Tropospheric Clouds, *Bull. Amer. Meteor. Soc.* 86(6):795–806.
- Chen, B. T., and Yeh, H. C. (1987). An Improved Virtual Impactor: Design and Performance, *J. Aerosol Sci.* 18(2):203–214.
- Chen, J.-P., and Lamb, D. (1999). Simulation of Cloud Microphysical and Chemical Processes Using a Multicomponent Framework: Part II: Microphysical Evolution of a Wintertime Orographic Cloud, *J. Atmos. Sci.* 56:2293–2312.
- Collett Jr., J., Oberholzer, B., and Staehelin, J. (1993). Cloud Chemistry at MT Rigi, Switzerland: Dependence on Drop Size and Relationship to Precipitation Chemistry, *Atmos. Environ.* 27A(1):33–42.
- Connolly, P., Flynn, M., Ulanowski, Z., Choularton, T., and Gallagher, M. (2007). Calibration of 2-D Imaging Probes Using Calibration Beads and Ice Crystal Analogues. Part 1: The Depth-of-Field, *J. Atmos. Oceanic Technol.* in press.
- Cozic, J., Verheggen, B., Mertes, S., Connolly, P., Bower, K., Petzold, A., Baltensperger, U., and Weingartner, E. (2007). Scavenging of Black Carbon in Mixed Phase Clouds at the High Alpine Site Jungfraujoch, *Atmos. Chem. Phys.* 7:1797–1807.
- Cziczko, D. J., Murphy, D. M., Hudson, P. K., and Thompson, D. S. (2004). Single Particle Measurements of the Chemical Composition of Cirrus ice Residue During CRYSTAL-FACE, *J. Geophys. Res.* 109:doi:10.1029/2003JD004032.
- Diehl, K., Simmel, M., and Wurzler, S. (2006). Numerical Sensitivity Studies on the Impact of Aerosol Properties and Drop Freezing Modes on the Glaciation, Microphysics, and Dynamics of Clouds, *J. Geophys. Res.* 111(D7):D07202, doi:10.1029/2005JD005884.
- Ebert, M., Inerle-Hof, M., and Weinbruch, S. (2002). Environmental Scanning Electron Microscopy as a New Technique to Determine the Hygroscopic Behaviour of Individual Aerosol Particles, *Atmos. Environ.* 36:5909–5916.
- Fukuta, N., and Takahashi, T. (1999). The Growth of Atmospheric Ice Crystals: A Summary of Findings in Vertical Supercooled Cloud Tunnel Studies, *J. Atmos. Sci.* 56(12):1963–1979.
- Gardiner, B. A., and Hallett, J. (1985). Degradation of In-Cloud Forward Scattering Spectrometer Probe Measurements in the Presence of Ice Particles, *J. Atmos. Oceanic Technol.* 2:171–180.

- Gerber, H. (1991). Direct Measurement of Suspended Particulate Volume Concentration and Far-Infrared Extinction Coefficient with a Laser-Diffraction Instrument, *Appl. Opt.* 30(33):4824–4831.
- Hallett, J., and Christensen, L. (1984). Splash and Penetration of Drops in Water, *Journal de Recherches Atmospheriques*. 18(4):226–262.
- Heintzenberg, J., Okada, K., and Ström, J. (1996). On the Composition of Non-Volatile Material in Upper Tropospheric Aerosols and Cirrus Crystals, *Atmos. Res.* 41:81–88.
- Henning, S., Bojinski, S., Diehl, K., Ghan, S., Nyeki, S., Weingartner, E., Wurzel, S., and Baltensperger, U. (2004). Aerosol Partitioning in Natural Mixed-Phase Clouds, *Geophys. Res. Lett.* 31:doi:10.1029/2003GL019025.
- Heymsfield, A. J., Bansemer, A., Schmitt, C., Twohy, C., and Poellot, M. R. (2004). Effective ice Particle Densities Derived from Aircraft Data, *J. Atmos. Sci.* 61:982–1003.
- Jayne, J. T., Leard, D. C., Zhang, X., Davidovits, P., Smith, K. A., Kolb, C. E., and Worsnop, D. R. (2000). Development of an Aerosol Mass Spectrometer for Size and Composition Analysis of Submicron Particles, *Aerosol Sci. Technol.* 33:49–70.
- Korolev, A., and Isaac, G. (2003). Roundness and Aspect Ratio of Particles in Ice Clouds, *J. Atmos. Sci.* 60(15):1795–1808.
- Korolev, A., and Isaac, G. A. (2005). Shattering During Sampling by OAPs and HVPS. Part I: Snow Particles, *J. Atmos. Oceanic Technol.* 22:528–542.
- Korolev, A., Isaac, G., Cober, S. G., Strapp, J. W., and Hallett, J. (2003). Microphysical Characterization of Mixed-Phase Clouds, *Q. J. Roy. Meteor. Soc.* 129(587):39–65.
- Laj, P., Flossman, A. I., Wobrock, W., Fuzzi, S., Orsi, G., Ricci, L., Mertes, S., Schwarzenböck, A., Heintzenberg, J., and Ten Brink, H. (2001). Behavior of H<sub>2</sub>O<sub>2</sub>, NH<sub>3</sub>, and Black Carbon in Mixed Phase Clouds During CIME, *Atmos. Res.* 58(4):315–336.
- Lawson, R. P., Baker, B. A., Schmitt, C. G., and Jensen, T. L. (2001). An Overview of Microphysical Properties of Arctic Clouds Observed in May in July 1998 During FIRE ACE, *J. Geophys. Res.* 106(D14):14989–15014.
- Linke, C., Möhler, O., Veres, A., Mehásci, Á., Bozóki, Z., Szabó, G., and Schnaiter, M. (2006). Optical Properties and Mineralogical Composition of Different Saharan Mineral Dust Samples: A Laboratory Study, *Atmos. Chem. Phys.* 6:3315–3323.
- Lohmann, U., and Feichter, J. (2005). Global Indirect Aerosol Effects: A Review, *Atmos. Chem. Phys.* 5:715–737.
- Mertes, S., Lehmann, K., Nowak, A., Massling, A., and Wiedensohler, A. (2005). Link Between Aerosol Hygroscopic Growth and Droplet Activation Observed for Hill-Capped Clouds at Connected Flow Conditions During FEBUKO, *Atmos. Environ.* 39(23–24):4247–4256.
- Mertes, S., Schwarzenböck, A., Laj, P., Wobrock, W., Pichon, J. M., Orsi, G., and Heintzenberg, J. (2001). Changes of Cloud Microphysical Properties During the Transition from Supercooled to Mixed-Phase Conditions During CIME, *Atmos. Res.* 58(4):267–294.
- Murphy, D. M., Cziczo, D. J., Hudson, P. K., Thomson, D. S., Wilson, J. C., Kojima, T., and Buseck, P. R. (2004). Particle Generation and Resuspension in Aircraft Inlets When Flying in Clouds, *Aerosol Sci. Technol.* 38:400–408.
- Noone, K. J., Hansson, H.-C., and Mallant, R. K. A. M. (1992). Droplet Sampling from Crosswinds: An Inlet Efficiency Calibration, *J. Aerosol Sci.* 23(2):153–164.
- Ogren, J. A., Heintzenberg, J., and Charlson, R. J. (1985). In-Situ Sampling of Clouds with a Droplet to Aerosol Converter, *Geophys. Res. Lett.* 12(3):121–124.
- Oshchepkov, S., Isaka, H., Gayet, J.-F., Sinyuk, A., Auriol, F., and Havemann, S. (2000). Microphysical Properties of Mixed-Phase & Ice Clouds Retrieved from In Situ Airborne “Polar Nephelometer” Measurements, *Geophys. Res. Lett.* 27(2):209–212.
- Rogers, R. R., and Yau, M. K. (1991), *A Short Course in Cloud Physics*. Pergamon Press, Oxford.
- Sassen, K., DeMott, P. J., Prospero, J. M., and Poellot, M. R. (2003). Saharan Dust Storms and Indirect Aerosol Effects on clouds: CRYSTAL-FACE results, *Geophys. Res. Lett.* 30(12):doi:10.1029/2003GL017371, 35-1-35-4.
- Schneider, J., Hings, S., Hock, N., Weimer, S., Borrmann, S., Fiebig, M., Petzold, A., Busen, R., and Kärcher, B. (2006). Aircraft-Based Operation of an Aerosol Mass Spectrometer: Measurements of Tropospheric Aerosol Composition, *J. Aerosol Sci.* 37:839–857.
- Schwarzenböck, A., Heintzenberg, J., and Mertes, S. (2000). Incorporation of Aerosol Particles Between 25 and 850 Nanometers into Cloud Elements: Measurement with a New Complementary Sampling System, *Atmos. Res.* 52(4):241–260.
- Schwarzenböck, A., Mertes, S., Heintzenberg, J., Wobrock, W., and Laj, P. (2001). Impact of the Bergeron Findeisen Process on the Release of Aerosol Particles During the Evolution of Cloud Ice, *Atmos. Res.* 58(4):295–313.
- Seifert, M., Ström, J., Krejci, R., Minikin, A., Petzold, A., Gayet, J.-F., Schumann, U., and Ovarlez, J. (2003). In-situ Observations of Aerosol Particles Remaining from Evaporated Cirrus Crystals: Comparing Clean and Polluted Air Masses, *Atmos. Chem. Phys.* 3:1037–1049.
- Seifert, M., Ström, J., Krejci, R., Minikin, A., Petzold, A., Gayet, J. F., Schlager, H., Ziereis, H., Schumann, U., and Ovarlez, H. (2004). Thermal Stability Analysis of Particles Incorporated in Cirrus Crystals and of Non-Activated Particles in Between the Cirrus Crystals: Comparing Clean and Polluted Air Masses, *Atmos. Chem. Phys.* 4:1343–1353.
- Straub, D. J., and Collett, J. J. L. (2001). Numerical and Experimental Performance Evaluation of the 3-Stage FROSTY Supercooled Cloud Collector, *Aerosol Sci. Technol.* 34(3):247–261.
- Ström, J., and Ohlsson, S. (1998). Real-Time Measurement of Absorbing Material in Contrail Ice Using a Counterflow Virtual Impactor, *J. Geophys. Res.* 103(D8):8737–8741.
- Sun, Z., and Shine, K. P. (1995). Parameterization of Ice Cloud Radiative Properties and its Application to the Potential Climatic Importance of Mixed-Phase Clouds, *J. Clim.* 8(7):1874–1888.
- Tenberken-Pötzsch, B., Schwikowski, M., and Gäggeler, H. W. (2000). A method to Sample and Separate Ice Crystals and Supercooled Cloud Droplets in Mixed Phased Clouds for Subsequent Chemical Analysis, *Atmos. Environ.* 34:3629–3633.
- Turner, D. D. (2005). Arctic Mixed-Phase Cloud Properties from AERI Lidar Observations: Algorithm and Results from SHEBA, *J. Appl. Meteorol.* 44:427–444.
- Twohy, C. H., and Gandrud, B. W. (1998). Electron Microscope Analysis of Residual Particles from Aircraft Contrails, *Geophys. Res. Lett.* 25(9):1359–1362.
- Twohy, C. H., and Poellot, M. R. (2005). Chemical Characteristics of Ice Residual Nuclei in Anvil Cirrus Clouds: Evidence for Homogeneous and Heterogeneous Ice Formation, *Atmos. Chem. Phys.* 5:2289–2297.
- Vali, G. (1996). Ice Nucleation—A Review. in *Nucleation and Atmospheric Aerosols 1996*, M. Kulmala and P. E. Wagner, eds., Elsevier, Oxford, 271–279.
- Verheggen, B., Cozic, J., Weingartner, E., Mertes, S., Bower, K., Flynn, M., Connolly, P., Gallagher, M., and Baltensperger, U. (2007). Aerosol Activation in Liquid and Mixed Phase Clouds at the High Alpine Site Jungfraujoch, *J. Geophys. Res.* submitted.
- Vidaurre, G., and Hallett, J. (2006). *Energetics of mixed phase cloud particle interactions*. 12th Conference on clouds physics. American Meteorological Society. Madison, Wisconsin, 10–14 July 2006.
- Walter, S., Schneider, J., Hock, N., Curtius, J., Borrmann, S., Mertes, S., Weingartner, E., Verheggen, B., Cozic, J., and Baltensperger, U. (2006). Mass Spectrometric Analysis of Residuals from Small Ice Particles and Supercooled Droplets During CLACE, *Atmos. Chem. Phys.* in preparation.
- Weingartner, E., Nyeki, S., and Baltensperger, U. (1999). Seasonal and Diurnal Variation of Aerosol Size Distributions (10 < D < 750 nm) at a High-Alpine Site (Jungfraujoch 3580 m asl), *J. Geophys. Res.* 104(D21):26809–26820.